cosmetics

MDPI

Article

Comparative Effects of Botulinum Toxin A, α-Bungarotoxin, Myricetin, and a Natural Extract Blend on Neurotransmitter Levels and Gene Expression in Human Skin Explants

Hyeyoun Kim [1], Franck Juchaux [2], Sabrine Benosmane [2], Jin-Woo Min [3], Young Mok Heo [1], Younhwa Nho [1], Chan-Yeong Heo [4], Dong-Geol Lee [1], Chunho Park [1], Seunghyun Kang [5], Richard J. Betts [6,*] and Ryang Yeo Kim [7]

[1] Research and Innovation Center, Cosmax BTI, Seongnam 13486, Republic of Korea; hyeyoun@cosmax.com (H.K.)
[2] L'Oréal Research & Innovation, 93601 Aulnay-Sous-Bois, France; franck.juchaux@loreal.com (F.J.); sabrine.benosmane@loreal.com (S.B.)
[3] GFC Life Science Co, Ltd., Hwaseong 18471, Republic of Korea
[4] Department of Plastic Surgery Seoul National University Bundang Hospital, Seongnam 13620, Republic of Korea
[5] Research and Innovation Center, Cosmax, Seongnam 13486, Republic of Korea; shyunk@cosmax.com
[6] L'Oréal Research & Innovation, Singapore 048583, Singapore
[7] L'Oréal Research & Innovation, Korea Innovation Centre, Seoul 06164, Republic of Korea; ryangyeo.kim@loreal.com
* Correspondence: richard.betts@loreal.com

Abstract

Injected botulinum neurotoxins (BoNT) reduce dynamic wrinkles by cleaving SNARE proteins at the neuromuscular junction; however, their large size mostly limits their use to injectable procedures. Certain polyphenols, including myricetin, have been shown in neuronal systems to reduce acetylcholine (ACh)-induced muscle contraction via inhibition of SNARE complex zippering, suggesting potential for topical use as modulators of skin cholinergic activity. This study aimed to identify a natural extract blend similarly capable of reducing ACh levels, followed by characterization of the activity of this extract on human skin explants, alongside reference molecules BoNT/A, α-bungarotoxin, and myricetin. The natural extract blend ("Blend 1") inhibited vesicle fusion and attenuated norepinephrine release in a cell culture system, inhibited muscle cell contraction within nerve/muscle co-culture, and reduced ACh levels consistent with myricetin and reference neurotoxins within human skin explants. Bulk transcriptomics of treated ex vivo skin explants revealed that BoNT/A, myricetin, and Blend 1 all shared a similar downregulated inflammatory and antiviral gene profile separate from α-bungarotoxin, but that myricetin and Blend 1 shared a large degree of overlap for upregulated genes associated with skin homeostasis and repair that was not observed for either toxin. These data support Blend 1 as a candidate for topical cosmetic use through modulation of BoNT/A-like cholinergic pathways, alongside activation of additional pathways associated with skin homeostasis and repair.

Keywords: botulinum toxin type A; myricetin; polyphenol; SNARE complex; acetylcholine; ex vivo human skin explant; bulk transcriptomics; neurocutaneous; topical cosmetic ingredient

Check for updates

Academic Editor: Enzo Berardesca

Received: 8 September 2026
Revised: 23 October 2026
Accepted: 24 October 2026
Published: 28 October 2026

Copyright: © 2026 by the authors. Licensee MDPI, Basel, Switzerland. This article is an open access article distributed under the terms and conditions of the Creative Commons Attribution (CC BY) license.

1. Introduction

The primary layers of the skin, the stratum corneum, epidermis, and dermis, are subject to the natural process of chronological aging, and extrinsic exposome factors such as UV and

pollution, which promote skin aging. While changes to these skin layers lead to commonly observed signs of aging such as uneven skin tone and wrinkling, the deeper parts of the skin such as the hypodermis and the underlying skeletal muscle also have critical contributions to skin appearance. Broader changes in skin and facial appearance with age, such as skin laxity and deeper wrinkles, are more a consequence of changes in hypodermis fat quality and basal muscle tone than changes in the more superficial skin layers, and as such are a common target for anti-aging procedures.

One of the most common and effective anti-aging cosmetic procedures is the injection of botulinum neurotoxins (BoNT), widely known by trade names such as Botox. Botulinum neurotoxins enter the motor nerve terminals at the neuromuscular junction via receptor-mediated endocytosis, where endosome acidification promotes translocation of the BoNT light chain into the neuronal cytosol, while reduction of the disulfide bond linking the heavy and light chains allows the light chain to be released from the heavy chain [1]. The light chain is then able to inhibit the neuronal soluble N-ethylmaleimide-sensitive factor attachment protein receptor (SNARE) complex, which consists of vesicle-associated membrane protein 2 (VAMP2) on the vesicle membrane, and syntaxin-1 and SNAP-25 on the neuronal plasma membrane. To initiate the process of fusion, these proteins interact to form the parallel four-helix protein bundle SNARE complex [2]. While there are various hypotheses to explain subsequent events, the prevailing model is for a zippering process whereby the complex forms at the N-terminus and progressively zips toward the membranes, allowing the membranes of the vesicle and neuron to come sufficiently close to initiate fusion pore opening, allowing for the release of vesicle contents across the synaptic cleft [3]. Different BoNT serotypes can target different parts of the SNARE complex; BoNT serotypes A, C, and E all cleave SNAP-25, with BoNT/C also able to cleave syntaxin-1; BoNT serotypes B, D, F, and G act on the vesicle-associated VAMP2/synaptobrevin [4]. Of these BoNT serotypes, it is BoNT/A that is commonly used within medical aesthetics clinics. The SNARE inhibition-induced inhibition of ACh release by BoNT results in paralysis of the affected muscles, leading to a reduction in wrinkle magnitude when used clinically.

While the clinical efficacy of BoNT/A has led to its widespread adoption within the medical aesthetics industry, the cost and invasive requirement for injections by well-trained medical practitioners reduce patient accessibility. There has therefore been considerable research into potential alternatives focused on peptides and molecules from natural sources that have lower molecular weights and more favorable skin penetration profiles. One molecular family of particular interest is polyphenols, a structurally diverse family of naturally occurring phenols with a history of safe use in cosmetics [5]. Yang and colleagues screened a panel of 39 polyphenolic compounds for their ability to prevent SNARE complex formation and vesicle membrane fusion, identifying several structures capable of preventing SNARE-mediated fusion and thus potentially possessing similar biological activity to BoNT/A family proteins [6]. In contrast to the irreversible cleavage of SNAP proteins (specifically SNAP-25) by BoNT/A, these polyphenols act by preventing SNARE zippering, albeit via slightly different mechanisms. Delphinidin and cyanidin inhibit the N-terminal nucleation of the SNARE complex independently of Ca^{2+} [7], in contrast to myricetin, which binds to the middle region of the SNARE complex, arresting the hemifusion process [6]. Myricetin, a flavonoid found within a diverse range of dietary sources, is of particular interest due to its low molecular weight and high efficacy within these neuronal cell culture systems [6]. Animal studies have demonstrated that injection of myricetin, as well as delphinidin and cyanidin, inhibits muscular contraction [8]. While the magnitude of this response was smaller compared to a reference BoNT/A, the onset of action was faster, a possible consequence of the lack of requirement for cellular processing as seen for BoNT/A, and there was no toxicity observed even at very high concentrations. These data suggest the potential

for natural products to mimic the effect of BoNT/A via similar mechanisms, but with a superior safety profile and in a reversible manner.

Within the present study, we aimed to explore topical alternatives to BoNT/A by examining the ability of myricetin and a natural extract blend containing myricetin and structurally similar polyphenols to inhibit neuromuscular contraction in line with a SNARE-mediated mechanism. We then extended these approaches to whole human skin, examining the impact of neurotoxin and natural extract treatment on ACh levels within ex vivo human skin explants, followed by characterization of the biological response of these compounds via bulk transcriptomics analysis.

2. Materials and Methods

2.1. Extract Materials and Extraction

The plant materials were selected on the basis of reported flavonol content, rather than on traditional or empirical cosmetic use. We selected myricetin as a reference starting point and positive control in much of our study; its interaction with the SNARE complex is the best characterized of the polyphenols identified to date. Our primary source for initial plant material selection was the survey of Miean and Mohamed [9]. They quantified myricetin and four other flavonoids across 62 edible tropical plants. Species in which myricetin was reported were prioritized. The selection was then extended to include further flavonol-rich sources. The plant materials used in this study included the fruits and leaves of guava (*Psidium guajava*), the bulbs of garlic (*Allium sativum*), the fruits of luffa (*Luffa cylindrica*), the leaves of black tea (*Camellia sinensis*), and the flowers of white water lily (*Nymphaea alba*). Each material was washed thoroughly with purified water, dried, and pulverized into particles ranging from 0.1 to 3 mm in size using a laboratory mill.

For each dried sample, purified water was added at a ratio of 1:100 (*w*/*v*), and the mixture was extracted with continuous stirring at room temperature for 3 days. The extract was filtered through Whatman No. 2 filter paper, and the remaining residue was subjected to the identical extraction and filtration procedure two additional times. Each filtrate was held at 4 °C until the three extraction cycles were complete. The combined filtrates were concentrated under reduced pressure using a rotary evaporator (Eyela, Tokyo, Japan) and lyophilized using a freeze dryer to yield dry powders of each respective plant extract. Microbial limits testing of the lyophilized extracts for total aerobic bacteria and fungi confirmed counts within the acceptance criteria applied to cosmetic raw materials.

2.2. Preparation of the Complex Extract Blends

To formulate the complex extract, the five individual plant extracts were precisely weighed and combined in specific proprietary proportions based on their respective extraction yields, generating five candidate blends (Blends 1–5) that differ from one another only in the relative ratio of the five constituent extracts. Each mixture was thoroughly homogenized to ensure uniformity and stored at −20 °C until further use in the cellular assays. The five candidate blends were screened in the membrane fusion and norepinephrine secretion assays described in Sections 2.3 and 2.4, and the best-performing blend, designated Blend1, was carried forward into all subsequent experiments.

2.3. Membrane Fusion Quantification

The inhibitory effects of test compounds on SNARE-mediated membrane fusion were evaluated using an in vitro FRET-based lipid-mixing assay. To prepare the assay components, recombinant SNARE proteins (SNAP-25, Syntaxin 1A, and VAMP-2) were expressed in *Escherichia coli Rosetta* (DE3), purified via glutathione agarose affinity chromatography, and validated by SDS-PAGE. These proteins were then reconstituted into two distinct

populations of liposomes. Unlabeled t-vesicles (POPC/DOPS, 65:35 mol%; 50 mM lipid) were reconstituted with a pre-assembled binary t-SNARE complex (SNAP-25 and Syntaxin 1A, 1:1 molar ratio) at a 1:100 protein-to-lipid ratio. Fluorescently labeled v-vesicles (POPC/DOPS/NBD-PE/Rhodamine-PE, 62:35:1.5:1.5 mol%; 10 mM lipid) were reconstituted with VAMP-2 at a 1:50 ratio. Following extensive dialysis to remove unincorporated proteins, the v-vesicles and t-vesicles were mixed at a 1:9 volume ratio in the presence or absence of the test samples. The fusion reaction was continuously monitored in independent triplicates at 37 °C for 90–120 min using a SpectraMax M2 multimode microplate reader (Molecular Devices, San Jose, CA, USA). The NBD-PE donor was excited at 465 nm (emission 530 nm), and the Rhodamine-PE acceptor emission was simultaneously recorded at 625 nm.

2.4. PC12 Cell Neurotransmitter (Norepinephrine) Secretion Quantification

PC12 cells were seeded at a density of 1×10^5 cells/well in type IV collagen-coated 24-well plates. To induce neuronal differentiation, cells were cultured in low-serum DMEM (1% horse serum) supplemented with 50 ng/mL nerve growth factor (NGF) for 5–7 days until neurite outgrowth was confirmed. For the secretion assay, differentiated cells were washed and pre-incubated in Locke's buffer (154 mM NaCl, 5.6 mM KCl, 3.6 mM $NaHCO_3$, 5.6 mM glucose, 0.1% BSA, pH 7.4) for 15 min at 37 °C. Cells were then treated with test samples for 30 min, followed by stimulation with NGF (50 ng/mL) in Locke's solution for an additional 15 min. Conditioned media were collected, centrifuged at 300× *g* for 5 min to remove cellular debris, and analyzed using a Norepinephrine ELISA kit (Abcam, Cambridge, UK, Cat No. ab287789) according to the manufacturer's instructions. Absorbance was measured at 450 nm using a microplate reader, and the percentage of inhibition was calculated relative to the NGF-stimulated control. Each condition was assayed in three independent wells.

2.5. Nerve and Muscle Cell Depolarization Co-Culture Evaluation

Human skeletal muscle cells (Lonza, Basel, Switzerland) were seeded in flasks as previously published [10] and maintained and cultivated with SkGM-2 skeletal Muscle Cell Growth Medium BulletKit (Lonza, Basel, Switzerland) as per the manufacturer's instructions. When cells reached about 80% confluency, muscle cells were transferred to 96-well plates in the proliferation medium. After 7 days of incubation, the medium was changed to differentiation medium. Under these conditions, muscle cells form fibers. The correct formation of fibers was validated morphologically before proceeding to the co-culture step. Motor neurons derived from hiPS cells of commercial origin were thawed and transferred into 96-well plates containing muscle cells in a medium containing 2/3rds of motor neurons commercial medium (iCell Motor Neuron Kit, Fujifilm Cellular Dynamics; Madison WI, USA) and 1/3rds of muscle differentiation medium. The co-culture was maintained for 10 days, and the culture medium was changed every two or three days. In these conditions, motor neurons mature and form junctions with muscle fibers. Spontaneous contractions were observed within 5 days. Co-culture was observed, and localization of contractile muscle fibers was registered. Movies of co-culture were recorded during 1 min before treatment with an In Cell 2200 automated microscope (General Electric, Boston, MA, USA). Cell cultures were then treated with the reference compound α-bungarotoxin at 2 μM or indicated compounds, and contractions were recorded for 2 min. The cultures were then incubated again at 37 °C and 5% CO_2 for 2 or 24 h before a further 2 min recording. The contraction frequency was then calculated from the 2 min recording. Six replicates were analyzed per condition. Data are representative of two independent experiments.

2.6. Skin Explant Source and Ethical Approval

Human skin was obtained from female donors immediately after abdominal or breast surgery, following written informed consent. Ethical approval for this study was granted by the Institutional Review Board (IRB) of Seoul National University Bundang Hospital (Seongnam, Republic of Korea; approval number B-2201-732-302), and all procedures were conducted in accordance with the Declaration of Helsinki.

2.7. Skin Explant Culture and Treatment

Upon collection, the explants were cultured in Dulbecco's Modified Eagle Medium (DMEM) supplemented with 10% fetal bovine serum (FBS), 1% antibiotics, 10 µg/mL insulin, 10 ng/mL hydrocortisone, and 2 mM L-glutamine. The explants were maintained at 37 °C in a humidified atmosphere of 5% CO_2.

For pharmacological treatments, the explants were treated with botulinum toxin type A (Hugel, Chuncheon, Republic of Korea) at 1 and 10 U/mL, α-bungarotoxin (Sigma-Aldrich, St. Louis, MO, USA) at 1 and 3 µM, Blend 1 at 5 and 15 µg/mL, or myricetin at 0.45 and 4.5 µg/mL. The treatments were administered by replacing the culture medium with fresh medium containing the respective agents once daily for three consecutive days. Untreated explants served as controls. An overview of the assays and treatments evaluated in this study is provided in Table 1.

Table 1. Overview of experimental assays and treatments evaluated. ✓ indicates that the treatment or screening material was evaluated in the specified assay, while—indicates that it was not evaluated. Initial screening experiments assessed natural extract blends, including what would later be termed Blend 1, whereas subsequent experiments evaluated the specified individual substances and Blend 1. This study was an international collaboration; therefore, BoNT/A was not available for the nerve–muscle co-culture experiments due to local legal restrictions.

Experiment/Endpoint	Natural Extract Blends (Including Blend 1)	BoNT/A	α-Bungarotoxin	Myricetin	Blend 1
Initial fusion screening	✓	–	–	–	–
Initial norepinephrine screening	✓	–	–	–	–
Nerve–muscle cell co-culture: contraction frequency	–	–	✓	✓	✓
Ex vivo human skin explants: ACh levels	–	✓	✓	✓	✓
Ex vivo human skin explants: bulk mRNA transcriptomics	–	✓	✓	✓	✓

For acetylcholine quantification, three explants per treatment condition were obtained from a single donor ($n = 3$), and the experiment was independently repeated three times. For bulk transcriptomics, independent skin samples from nine different donors were used (biological replicates, $n = 9$), processed in three independent experimental runs (three donors per run).

2.8. Acetylcholine Quantification

Following the treatments, the explants were washed with ice-cold PBS and homogenized in the assay buffer provided in the Choline/Acetylcholine Assay Kit (Abcam, Cambridge, UK, Cat No. ab65345). The tissue homogenates were centrifuged at 13,523× *g* for 5 min at 4 °C to pellet the cellular debris. The resulting supernatants were collected and

subjected to acetylcholine quantification strictly following the manufacturer's protocol. Fluorescence intensity was measured at Ex/Em = 535/587 nm using a SpectraMax M2 multimode microplate reader. The acetylcholine concentrations were extrapolated using a standard curve generated concurrently from six choline standards spanning 0–500 pmol/well, prepared for each assay according to the manufacturer's protocol. To account for variations in tissue size, the measured acetylcholine levels were normalized to the total protein concentration of each sample, which was determined using a BCA protein assay kit. Measurements therefore represent total tissue ACh content, encompassing vesicular, cytosolic, and extracellular pools. Each explant sample was assayed in triplicate for both acetylcholine and total protein.

2.9. Bulk Transcriptomics of Human Skin Explants

Human skin explants were treated with the respective compounds or an untreated control for three days. The experiment comprised five groups (one untreated and four treatment groups). The entire experiment was independently repeated three times, each with skin samples from three different donors, resulting in nine biological replicates ($n = 9$) per group and a total of 45 samples. Following the treatments, the explants were rinsed with ice-cold PBS, immediately immersed in RNAlater stabilization solution (AM7020), and shipped to Macrogen (Seoul, Republic of Korea). Total RNA extraction, library construction, and sequencing were performed by Macrogen using their standard protocols. RNA quality and quantity were evaluated using an Agilent 2100 Bioanalyzer (Agilent Technologies, Santa Clara, CA, USA), and only samples exhibiting an RNA integrity number (RIN) > 7.0 were utilized for library preparation.

Sequencing libraries were prepared using the TruSeq Stranded mRNA Library Prep Kit (Illumina, San Diego, CA, USA), and sequencing was subsequently performed on an Illumina NovaSeq X platform to generate 150 bp paired-end reads. For transcriptomic data analysis, raw sequencing reads were quality-checked, aligned to the human reference genome (GRCh38), and quantified using Macrogen's standard bioinformatics pipeline. For data pre-processing, low-expressed genes were filtered out to improve statistical power. Normalization and differential expression analysis were subsequently performed using DESeq2, which internally applies median-of-ratios normalization.

Differentially expressed genes (DEGs) between the treated and untreated control groups were identified using the negative binomial Wald test (nbinomWaldTest) via the DESeq2 R package, with sequencing batch included as a covariate in the design formula (~batch + treatment) to account for potential batch effects. Genes satisfying the criteria of Log2 fold change > 0.585 and adjusted p-value < 0.05 were considered statistically significant. Gene Ontology (GO) enrichment analysis and network analysis of the identified DEGs were conducted using the STRING Database v12.5 (https://string-db.org/, accessed on 12 October 2026). Inclusive DEG pairings between treatment groups are presented in a table, while exclusive DEG pairings are presented in UpSet plots. The gene counts reported in the Results are inclusive pairwise overlaps (Tables S5 and S6), rather than the exclusive intersection sizes shown in the UpSet plots (Section 3.4). Volcano plots were created using BioSketchArt Volcano Plot Maker (https://biosketch.art/volcano-plot, accessed on 11 May 2026). The UpSet plots were created using ChiPlot tools (https://www.chiplot.online/upset_plot.html, accessed on 24 July 2026), and the heatmap was created using Heatmapper (https://heatmapper.ca/, accessed on 28 August 2026).

2.10. Statistical Analysis

Data from the membrane fusion, norepinephrine secretion, muscle contraction, and acetylcholine quantification assays are presented as the mean ± standard deviation unless

stated otherwise in the corresponding figure legend, and were compared using one-way ANOVA with Holm–Sidak correction for multiple comparisons against the respective control group. Normality of residuals and homogeneity of variances were assessed using the Shapiro–Wilk and Brown–Forsythe tests, respectively. Where variances were unequal (Section 3.2), Welch's ANOVA with Dunnett's T3 multiple comparisons was used. The number of replicates for each experiment is given in the corresponding figure legend. Differential expression analysis of the RNA sequencing data was performed as described in Section 2.9. A p-value < 0.05 was considered statistically significant. Statistical analyses were performed using GraphPad Prism version 11 (GraphPad Software, Boston, MA, USA).

3. Results

3.1. Natural Extract Blend Evaluation for Inhibition of Vesicle Fusion and Norepinephrine Release

Previous reports have indicated that myricetin inhibits vesicle fusion and norepinephrine (NE) release within cell systems; however, pure polyphenol structures are often not permissible for cosmetic use. To identify extracts with SNARE-inhibitory activity, we screened a series of preparations from natural sources that contain myricetin and associated polyphenolic structures and validated their biological activity for membrane fusion in a FRET-based lipid-mixing assay. Of the five candidate blends, Blend 1 inhibited membrane fusion to the greatest extent and did so in a dose-dependent manner (Figure 1A). As PC12 cells serve as a highly established in vitro model for studying SNARE-dependent exocytosis, we also examined NE secretion as a functional surrogate marker to evaluate general vesicle fusion inhibition, finding that Blend 1 gave the greatest inhibition of NE release (Figure 1B). These screening data identify Blend 1 as the most active of the five candidate ratios in both assays.

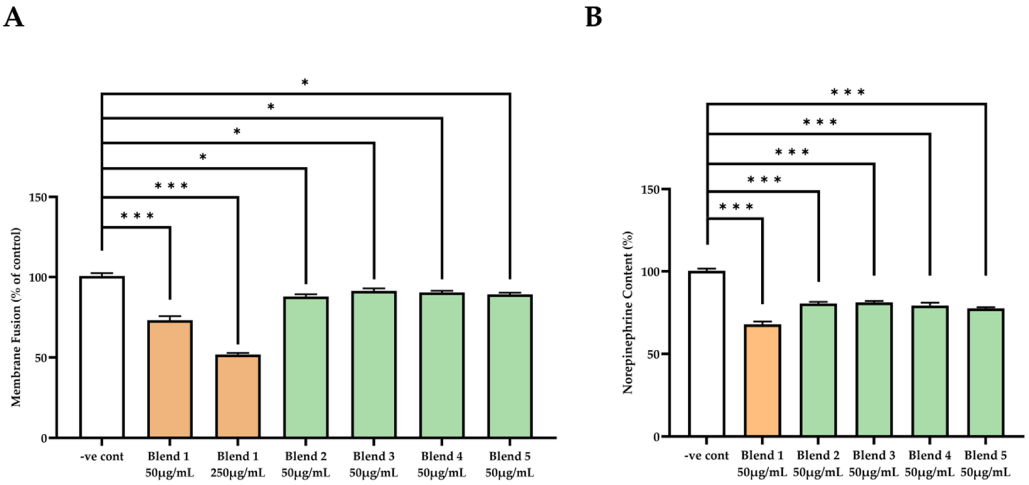


Figure 1. Screening of candidate polyphenol extract blends for inhibition of neurotransmitter vesicle fusion and norepinephrine release. Blends 1–5 comprise the same five plant extracts combined in different proportions. (**A**) Membrane fusion inhibition within a cell-free liposome FRET assay; Blend 1 was tested at two concentrations to establish dose-dependence and all other blends at 50 µg/mL. (**B**) Norepinephrine release was quantified to determine whether reduced fusion is concordant with a decrease in neurotransmitter levels; all blends were tested at 50 µg/mL, with the selected blend, Blend 1, highlighted in orange. All data represent the mean ± standard deviation; * denotes $p < 0.05$ and *** $p < 0.001$, one-way ANOVA with Holm–Šídák multiple comparisons against the negative control. $n = 3$ independent replicate wells per condition in each panel; data are representative of three individual experiments. One-way ANOVA: (**A**) $F(6,14) = 309.4$, $p < 0.0001$; (**B**) $F(5,12) = 194.8$, $p < 0.0001$.

3.2. Neurotoxins, Myricetin and Blend 1 Inhibit Muscle Cell Depolarization

Previous reports have demonstrated myricetin and similar polyphenol structures to inhibit presynaptic membrane fusion therefore reduce muscle contraction, so we examined the ability of both myricetin and natural extract to inhibit muscle contraction frequency within a co-culture system of iPSC-derived neurons and skeletal muscle cells. In this system, the neuronal cells self-arrange to form synaptic connections with the muscle cells, resulting in a basal level of muscle contraction. The cultures were treated with either positive control α-bungarotoxin, a competitive antagonist of the nicotinic acetylcholine receptor (nAChR), our reference polyphenol myricetin, or Blend 1. None of the compounds at any concentration tested showed any evidence of toxicity. When the cell cultures were treated for 2 h, only Blend 1 at the highest concentration tested showed a reduction in muscle contraction (Figure 2A). After 24 h post-treatment, however, all treatments examined exhibited a significant decrease in muscle contraction frequency, and in some cases, there was a near-complete abolition of muscle contraction, suggesting almost total inhibition of neuromuscular junction signaling (Figure 2B). These data are consistent with previous reports of myricetin inhibiting vesicle fusion, and demonstrate the same physiological properties for Blend 1.

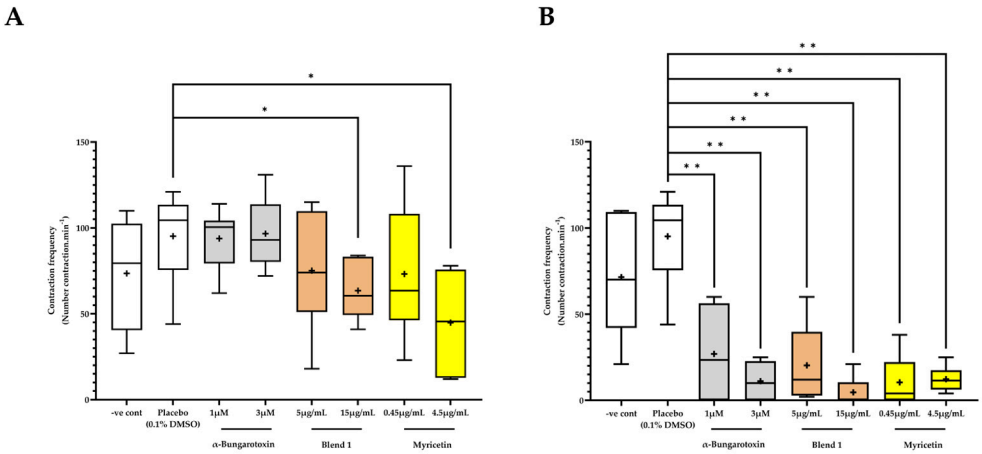


Figure 2. Neurotoxins and natural extracts inhibit the contraction frequency of skeletal muscle fibers within a muscle cell/nerve cell co-culture. Skeletal muscle and nerve cells were cultured in the presence of the indicated treatment for (**A**) 2 h or (**B**) 24 h, after which spontaneous contractions of the muscle cells were counted over a 2 min recording. Data are shown as box-and-whisker plots; boxes represent the interquartile range, the horizontal line indicates the median, the + symbol indicates the mean, and whiskers indicate the data range. Colors indicate treatment groups: white, vehicle control; gray, α-bungarotoxin; orange, Blend 1; yellow, myricetin. * denotes $p < 0.05$ and ** $p < 0.01$; $n = 6$. (**A**) One-way ANOVA with Holm–Šídák multiple comparisons against vehicle (0.1% DMSO) control. (**B**) Welch's ANOVA with Dunnett's T3 multiple comparisons against vehicle (0.1% DMSO) control. (**A**) $F(7,40) = 2.33$, $p = 0.043$; (**B**) $W(7, 16.80) = 8.78$, $p = 0.0001$.

3.3. BoNT/A, Myricetin and Blend 1 and Natural Extracts Reduce ACh Levels Within Human Skin Explants

We next examined if this mechanism extended into skin by targeting ACh, the primary physiological transmitter for muscle contraction. To this end, we established an ACh quantification assay system whereby human skin explants were cultured in media and treated with positive controls BoNT/A or α-bungarotoxin, and myricetin and Blend 1 for either a single treatment or three consecutive treatments, followed by ACh quantification within homogenized whole skin explants. Following a single-day treatment, we saw a decrease in ACh levels within cultures treated with either myricetin or Blend 1, but not BoNT/A or α-bungarotoxin (Figure 3A). However, when treatment was extended to three consecutive days, BoNT/A treatment resulted in a decrease in ACh, while both myricetin and Blend

1 continued to reduce ACh levels (Figure 3B). As anticipated, α-bungarotoxin did not decrease ACh levels, as this toxin acts postsynaptically on nicotinic ACh receptors rather than reducing ACh levels in the manner of BoNT/A. It increased ACh, however, which may be explained by a transient increase in ACh due to reduced α7-nAChR binding or dysregulated ACh release negative feedback. These data demonstrate that the mechanisms we see behind the reduction of muscle contraction observed within our study similarly extend to skin.

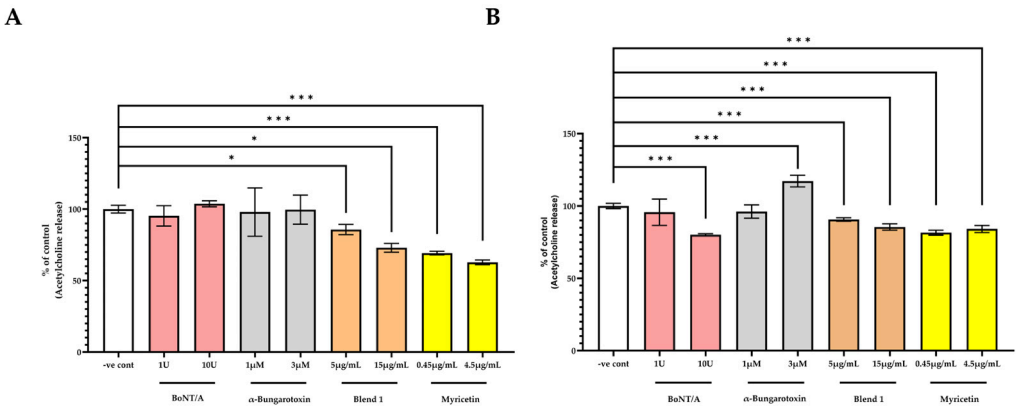


Figure 3. Neurotoxins and natural extracts modulate ACh levels within ex vivo human skin explants. Skin explants were treated for either a single day (**A**) or three consecutive days (**B**) with the indicated treatment conditions, after which the whole skin explants were homogenized and assayed for ACh levels. All data represent the mean ± standard deviation normalized to ACh readings for untreated skin samples. * denotes $p < 0.05$ and *** $p < 0.001$; $n = 3$ explants per condition from a single donor; data are representative of three independent experiments. One-way ANOVA with Holm–Šídák multiple comparisons against untreated control: (**A**) $F(8,18) = 101.4$, $p < 0.0001$; (**B**) $F(8,18) = 25.55$, $p < 0.0001$.

3.4. Ex Vivo Skin Explants Treated with BoNT/A, Myricetin, and Blend 1 Share Overlapping but Distinct Transcriptomic Profiles

Transcriptomic analysis of treated skin explants showed BoNT/A treatment induced 328 differentially expressed mRNAs (66 up, 262 down) compared to untreated explants (absolute log2 fold change > 0.585, adjusted p-value < 0.05), α-bungarotoxin 109 genes (38 up, 71 down), myricetin 439 genes (184 up, 255 down) and Blend 1 155 genes (107 up, 48 down) (Figure 4A–D). Gene Ontology enrichment analysis for BoNT/A-downregulated pathways revealed impact on pathways associated with viral processes and defense against viruses, consistent with dampening of virus-associated innate immune responses and a reduction of a basal inflammation/stress response state (Figure 5A; network analysis Figure S1). This may be particularly prominent within a skin explant system, where injury response and tissue stress may be enhanced. Such pathways have a strong neuronal component [11] that would be a natural target for BoNT/A-induced attenuation. Our α-bungarotoxin-treated explants, however, showed a very different transcriptomic signature, with pathways associated with vascular development and angiogenesis being downregulated (Figure 5B; network analysis Figure S2). Despite both agents acting on the neuromuscular junction, there was very limited overlap in downregulated genes, with only 3 of the 262 genes downregulated by BoNT/A also impacted by α-bungarotoxin treatment (Figure 4E and Table S5) and only a single upregulated gene shared between conditions (Figure 4F and Table S6). There were limited functional networks upregulated by BoNT/A treatment, precluding GO analysis and highlighting that BoNT/A treatment within skin explants at the time point measured was primarily suppressive. α-Bungarotoxin treatment upregulated processes associated with keratinization (Figure 5E), consistent with an impact on epidermal cornification.

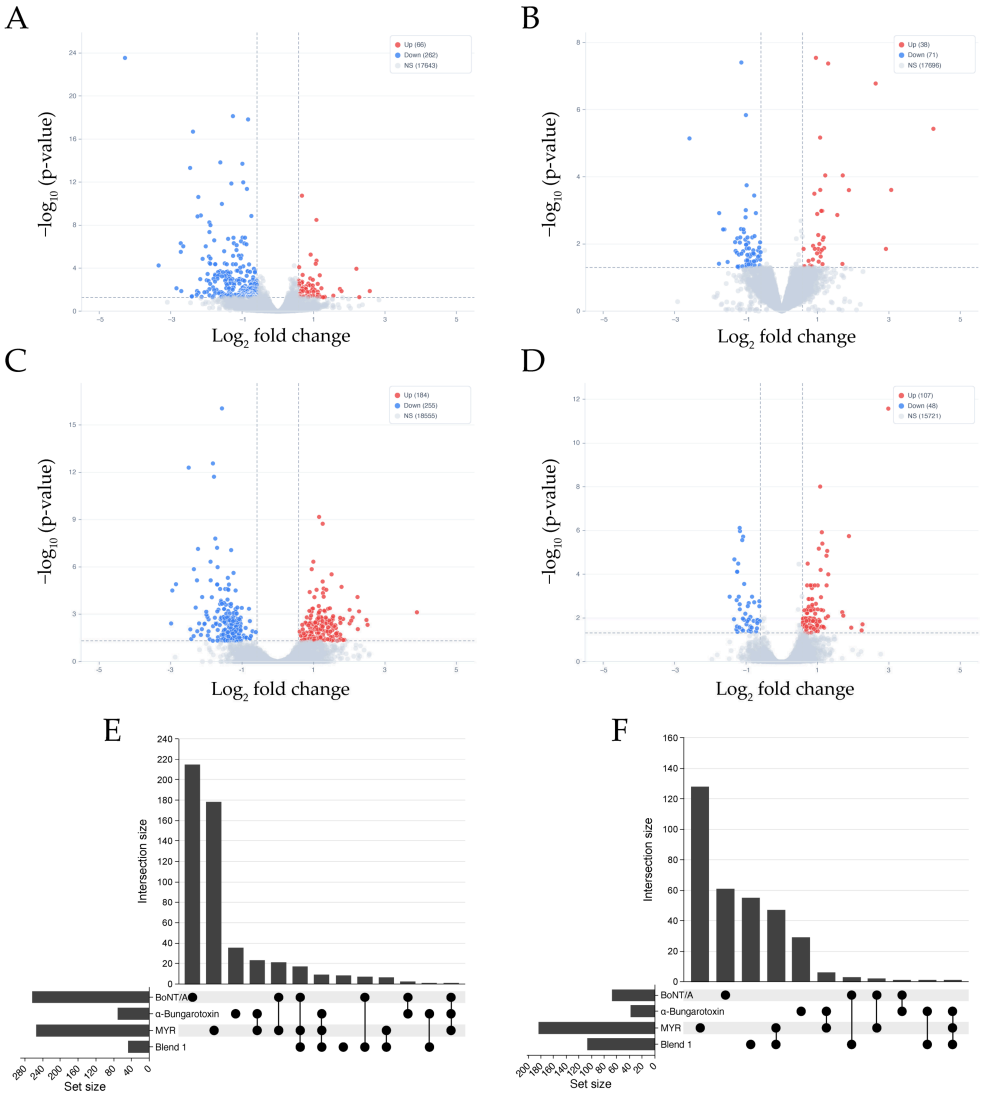


Figure 4. Neurotoxins and natural extracts have overlapping transcriptomic profiles within human skin explants. Skin explants were treated with the indicated conditions for three consecutive days, after which they were analyzed using bulk transcriptomics. Volcano plots for (**A**) BoNT/A, (**B**) α-bungarotoxin, (**C**) myricetin, and (**D**) Blend 1-treated samples. Genes significantly upregulated ($\log_2$FC > 0.585, adjusted p-value < 0.05) are marked in red, while those significantly downregulated ($\log_2$FC < −0.585, adjusted p-value < 0.05) are marked in blue. (**E**) UpSet plots showing downregulated and (**F**) upregulated differentially expressed genes across treatment groups, shown as exclusive intersections. Inclusive pairwise overlaps are given in Tables S5 and S6.

Treatment of skin explants with myricetin shared downregulated genes with both BoNT/A (39 of 255 genes) and α-bungarotoxin (33 of 255 genes)-treated samples (Figure 4E and Table S5). Myricetin-treated samples demonstrated significant similarities to α-bungarotoxin as demonstrated by GO analysis, with shared impact on vascular development and angiogenesis (Figure 5C; network analysis Figure S3). At the DEG level, however, myricetin shares a strong inflammatory/interferon-suppression core like BoNT/A-treated explants, including IFI44, IFI44L, ISG15, OAS2, CMPK2, MX1, HERC6, the seven interferon-stimulated genes subsequently used in the representative heatmap panel (Figure 6 and Table S7). Upregulated gene pathways were significantly different; however, myricetin treatment induced a broad program including epithelial-associated genes and stromal/remodeling-related transcripts such as FGF10, CXCL12, LYVE1, and THY1 (Figure 5F

and Table S3), compared to the keratinization signature of α-bungarotoxin (Figure 5E, network analysis Figure S2).

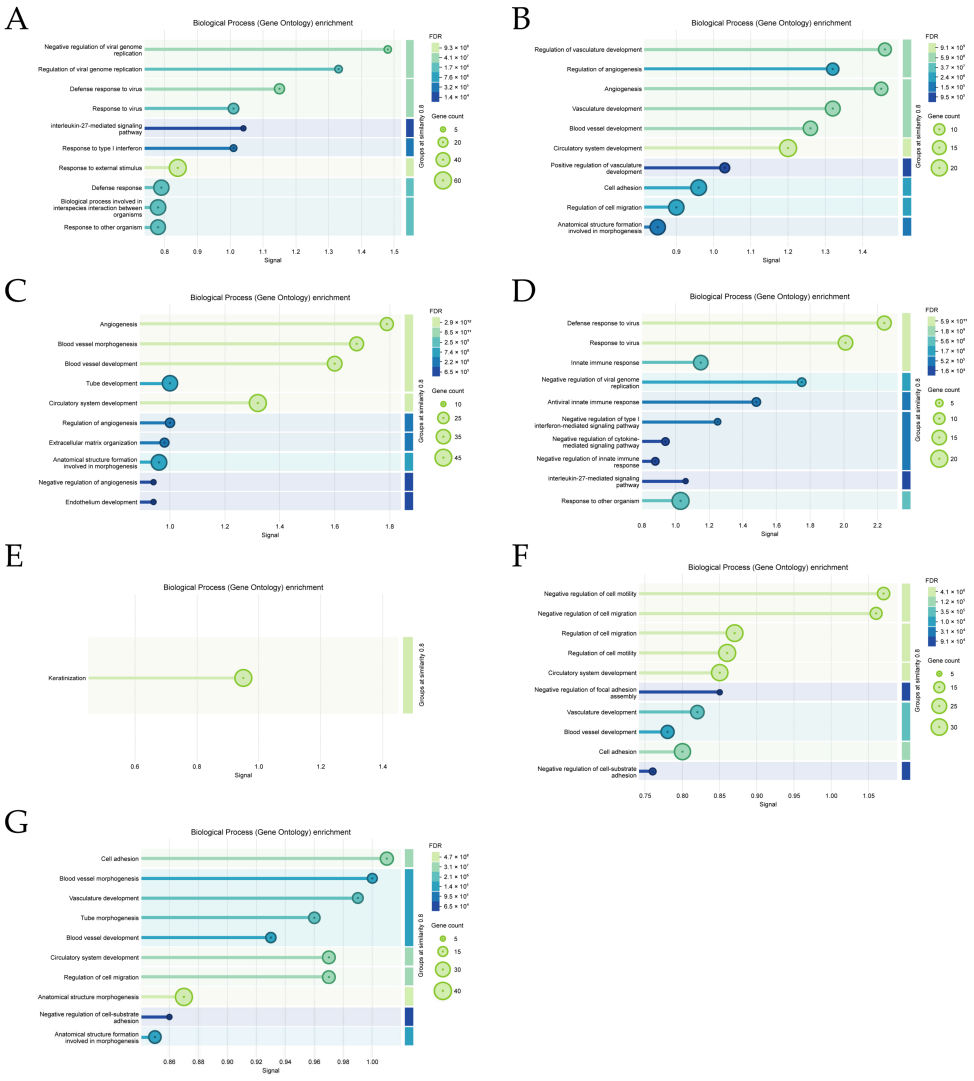


Figure 5. Neurotoxin and polyphenol treatments engage distinct pathway programs within ex vivo human skin explants. Gene Ontology enrichment for downregulated pathways following treatment with (**A**) BoNT/A, (**B**) α-bungarotoxin, (**C**) myricetin, and (**D**) Blend 1, and for upregulated pathways following treatment with (**E**) α-bungarotoxin, (**F**) myricetin, and (**G**) Blend 1. No significantly upregulated pathways were identified for BoNT/A-treated explants.

Blend 1 treatment shares considerable overlap with both BoNT/A and myricetin, with 17 of the 48 downregulated Blend 1 genes also being downregulated with both BoNT/A and myricetin (Figure 4E and Table S5). GO analysis similarly reveals a pathway modulation signature similar to BoNT/A, focused on defense response to virus and interferon-associated pathways (Figure 5D; network analysis Figure S4). The upregulated transcriptomic response was much more like myricetin than either BoNT/A or α -bungarotoxin, with 48 of the 107 genes upregulated by Blend 1 also impacted by myricetin, compared to only 2 genes shared with each of BoNT/A and α-bungarotoxin (Table S6 and Figure 4F). Of particular interest is Blend 1's impact on stromal/vascular remodeling genes such as FGF10, CXCL12, LYVE1, and THY1 (Figures 5G and S4), which are associated with skin homeostasis [12].

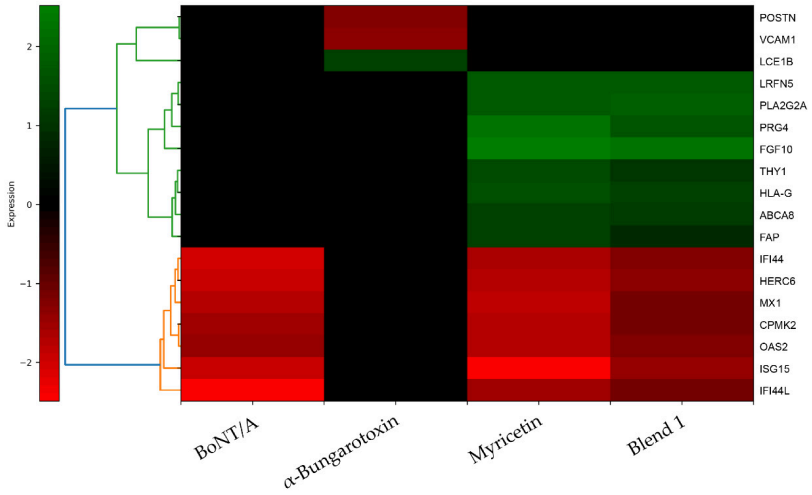


Figure 6. Heatmap of 18 representative differentially expressed genes across treatment groups. Rows represent indicated genes and columns represent treatment conditions. Colors represent Log2 fold change vs untreated control, with green indicating upregulation and red indicating downregulation. The dendrogram indicates hierarchical clustering of genes based on their expression profile using Euclidean distance.

To compare transcriptional responses across treatment groups, we generated a heatmap of 18 representative DEGs selected to capture three distinct biological programs (Figure 6 and Table S7). A cluster of seven interferon-stimulated genes (ISGs), including ISG15, IFI44, MX1, IFI44L, OAS2, CMPK2, and HERC6, were all downregulated in BoNT/A, myricetin-, and Blend 1-treated explants, defining a shared innate immune suppression signature. None of these seven ISGs were differentially expressed in α-bungarotoxin-treated explants (Table S2). In contrast, α-bungarotoxin showed a distinct response characterized by downregulation of VCAM1 and POSTN and upregulation of the terminal differentiation marker LCE1B, consistent with a postsynaptic response profile [13,14]. Myricetin and Blend 1 additionally shared upregulation of stromal and immune-associated genes, including FGF10, PRG4, and HLA-G, that were absent from both neurotoxin groups, defining a polyphenol-associated skin homeostasis and repair signature. Together, these patterns support the interpretation that BoNT/A, myricetin, and Blend 1 possess a shared inflammatory suppression program, whereas myricetin and Blend 1 additionally induce transcriptional responses in skin consistent with skin regeneration.

4. Discussion

Within the present study, we examined the ability of a natural polyphenol complex, polyphenol myricetin, and reference toxins to inhibit neural activation within an in vitro model of neuromuscular contraction and extended these findings to examine ACh levels within ex vivo skin. We also extended these data to transcriptomic signatures of these treatments within ex vivo skin explants. Our data support the potential for a natural extract preparation to improve skin quality not only via neuromuscular junction pathways, but likely through pathways independent of the neuromuscular junction.

The cholinergic system in skin is comprised of both neuronal and non-neuronal components. The sympathetic cholinergic nerve fibers of the skin neuronal system primarily act on the eccrine sweat glands but also influence the cutaneous vasculature and sensory C-fibers [15]. The non-neuronal cholinergic system is more extensive in skin and operates independently of neuronal inputs. Keratinocytes synthesize and release ACh, and express both nicotinic and muscarinic ACh receptors, which act in a mutually antagonistic manner to regulate cutaneous ACh function [16]. Fibroblasts express α7-nAChR, which regulates ECM

production and growth factor responsiveness [17]. Inhibition of nicotinic ACh receptors by a small peptide increased keratinocyte viability, further demonstrating the multifaceted nature of ACh within skin cells [18]. Cutaneous immune cells such as macrophages, T cells, and dendritic cells also express nAChRs. The ubiquity of cholinergic pathways in the skin makes it an interesting target for modulating skin quality and inflammatory responses by agents such as BoNT/A beyond utilization solely as injectables for anti-wrinkle activity.

Research into topical uses of BoNT/A has revealed promising results. A preparation of BoNT/A in a topical gel formulation reduced the prominence of lateral canthal area lines compared to the vehicle control in a randomized clinical study of 17–19 adult patients [19], while topical application of BoNT/A improved after ablative CO_2 fractional laser of lateral periorbital wrinkles compared to laser treatment alone within a small cohort of female patients [20]. The authors of this latter study note that in their previous pilot study topical BoNT/A alone had no effect, suggesting that enhanced delivery systems that improve skin penetration are likely to be extremely important given the very large size of BoNT/A proteins. This has led to recent studies examining the effect of topical BoNT/A in conjunction with microneedling to allow access of the BoNT/A protein into the epidermis and dermis. While these studies remain relatively small-scale, there is promising evidence for the use of topical BoNT/A in conjunction with microneedling or intradermal droplet injection for reducing crow's feet wrinkle appearance [21] and reducing atrophic post-acne scar appearance [22]. Nevertheless, the extremely large size of BoNT/A proteins has led to the development of smaller peptides to inhibit the SNARE complex. The most widespread example of this approach is that of hexapeptide Ac-EEMQRR-NH_2, commonly known by the brand name Argireline or acetyl hexapeptide-8. Argireline mimics the aa12-17 sequence of SNAP-25 and therefore blocks SNARE complex formation and resultant neurotransmitter release [23]. Dipeptide diaminobutyroyl benzylamide, more popularly known by its commercial trademark of Syn-ake®, was developed to possess the same biological activity as Waglerin-1, a protein originally isolated from viper venom which acts as a nicotinic ACh receptor antagonist [24]. Topical administration of Dipeptide diaminobutyroyl benzylamide in a formula with additional peptides and antioxidants improved skin wrinkling [25]. A similar approach has been taken using a neuromuscular Nav1.4 Na^+ channel-blocking μ-conotoxin [26]. Despite these impressive in vitro data and clinical results within small-scale trials, such peptides still have relatively high molecular weights. Within the present study, we examined natural structures and extracts with the aim of identifying solutions with potentially more favorable skin penetration profiles and that are from natural sources.

Our initial screens using a FRET-based lipid mixing assay and PC12 cell line indicated that Blend 1 of our extract gave the most promising results for SNARE inhibition as determined by attenuation of membrane fusion and NE release. We then utilized a more physiological system by co-culturing iPSC-derived motor neurons together with muscle cells to measure muscle contraction frequency as a direct functional assay for the consequences of ACh blockade. Our data demonstrate that both myricetin and Blend 1 extract inhibit muscle contraction in line with the results observed for α-bungarotoxin, consistent with the previously reported data for myricetin [6,8,27,28]. While these data suggest that myricetin contributes to the neuronal effects of Blend 1, such natural extract preparations are typically a complex mixture of structures and are likely to contain many different polyphenols. Indeed, myricetin is not the only flavonoid possessing the ability to inhibit SNARE zippering, as both delphinidin and cyanidin inhibit muscular contraction [8]. It is therefore possible that there are additional structures within our extract that contribute to the inhibition of muscle contraction we observed within our system.

While our data supports existing studies of the biological activity of polyphenols on neuromuscular junction activity inhibition, there have been limited studies to date

extending this approach specifically to skin. To examine the impact of our molecules of interest, we extended our study to human skin, measuring ACh levels within cultured human skin explants. The reduction of ACh levels within this system by both BoNT/A, myricetin, and Blend 1 is consistent with our data obtained within the neuronal system, suggesting that SNARE-mediated inhibition of vesicle fusion and the resultant decrease in neurotransmitter release are responsible for the inhibition of muscle cell depolarization within our system. These data are inconsistent with the findings of Schlereth and coworkers [29], who found that BoNT injected into the skin of volunteers did not result in a decrease in ACh levels as determined by HPLC analysis of dermal perfusion effluent that was run through the skin. They concluded that a significant proportion of the ACh they measured was from non-neuronal sources, and thus not impacted by BoNT inhibition of exocytotic ACh release. Our system is considerably different, however. We performed ACh quantification on whole skin homogenates, which capture whole skin ACh pools including vesicular and intracellular ACh, rather than only the extracellular fraction measured within the microdialysis. These considerable differences in experimental systems may explain our discordant results. Interestingly, bungarotoxin increased ACh within our skin explant system. We do not have data to explain this observation, although given the role of nAChR in ACh release regulation [30], interruption of feedback mechanisms regulating ACh release by blockade of AChRs by α-bungarotoxin would be consistent with our observations.

Having established the ability of our natural extract blend to modulate ACh levels, we wanted to examine the physiological consequences of these treatments within human skin via bulk transcriptomics. Our analysis revealed striking differences across treatment groups. At the timepoint measured, BoNT/A was predominantly suppressive, with substantially more downregulated than upregulated DEGs. GO analysis identified marked suppression of pathways related to antiviral defense and innate immune activation, particularly interferon-stimulated genes (ISGs). Although initially unexpected, this pattern may reflect the stressed nature of the ex vivo skin explant system, in which surgical excision and culture are likely to elevate basal inflammatory signaling. Under these conditions, compounds with anti-inflammatory or presynaptic inhibitory activity may reduce this background response. This interpretation is consistent with previous reports describing anti-inflammatory effects of BoNT/A through both neuronal and non-neuronal mechanisms [31,32]. Injection of BoNT/A resulted in a decrease in TNCB-induced inflammation within an animal model of atopic dermatitis [33], while BoNT/A treatment of rosacea patients resulted in clinically significant improvements in erythema scores [34]. This signature is shared with both myricetin and Blend 1, consistent with the shared presynaptic activity between both compounds and BoNT/A. SNARE family proteins VAMP-3, SNAP-29, and syntaxin-4 have all been implicated in cytokine release from primary human keratinocytes, with VAMP-3 identified as a target of particular interest for reducing inflammation within atopic dermatitis lesions [35]. These data all link the SNARE complex and therefore compounds that act on the complex to be associated with immune suppression. That α-bungarotoxin did not exhibit such an effect despite potent blockade of α7-nAChR suggests that the ISG arm of the cutaneous cholinergic system is mediated through an α7-nAChR-independent mechanism.

Where myricetin and Blend 1 diverge from BoNT/A is the upregulated DEG profile. BoNT/A treatment is overwhelmingly suppressive, with the large majority of its DEGs being downregulated, and it shares a limited upregulated gene signature with the polyphenol treatments. We observed 47 genes upregulated exclusively by myricetin and Blend 1, which are consistent with skin homeostasis and repair transcriptional programs that these polyphenols activate independent of their neuronal effects. This signature encompasses multiple aspects of skin tissue homeostasis and repair such as FGF10 and FAP (both implicated in fibroblast and keratinocyte signaling and tissue repair [36,37]), PRG4 (anti-fibrotic

ECM organization associated with dermal remodeling [38]), HLA-G (immune tolerance induction [39]), and THY1 (fibroblast activation, consistent with a pro-regenerative fibroblast state [40]). Myricetin protects against UV-B-induced damage and wrinkling in a mouse model of photoaging [41] and protects human keratinocytes from UV-B-induced photodamage [42], consistent with our observations. These data collectively indicate that myricetin and Blend 1 not only recapitulate the innate immune-suppressive signature of BoNT/A through their shared presynaptic cholinergic activity but also possess a skin homeostatic and repair program profile that BoNT/A does not. These dual pathways suggest these molecules may offer a functional advantage over BoNT/A for topical skin use.

A limitation of the present study is that the precise proportions in which the five constituent extracts are combined to form Blend 1 are proprietary and are not reported here, as the material is under commercial development. While the botanical sources and the full extraction protocol for each individual extract are given in Section 2.1, the undisclosed combining ratio does restrict direct independent replication of the results reported for Blend 1. An additional limitation is that our skin explants were obtained from female donors undergoing abdominal or breast surgery; the extent to which these findings generalize to male skin remains to be established. Finally, the study was limited to in vitro and ex vivo models; further study is required to determine the extent to which our data can translate clinically.

5. Conclusions

Within the present study, we conducted an initial screen of natural extract preparations to identify the most promising blend based on vesicle fusion and NE release. The most promising extract, which we termed Blend 1, was tested alongside reference molecules α-Bungarotoxin and myricetin, and we found that all inhibited muscle cell contraction in a nerve/muscle cell co-culture. We demonstrated that BoNT, myricetin, and Blend 1, but not α-bungarotoxin, reduced ACh levels within human ex vivo skin explants. We also identified a previously undescribed transcriptomic signature of human skin explants treated with BoNT/A involving viral defense and innate immune pathways, suggesting BoNT may have a more complex cutaneous profile than previously appreciated. This signature shares a partial overlap with the profiles observed following myricetin and Blend 1 treatment but not α-bungarotoxin, consistent with a shared modulation of neurocutaneous signaling. We also demonstrate that Blend 1 impacts additional transcriptomic pathways associated with skin homeostasis and repair-related processes beyond those shared with BoNT/A, collectively suggesting this extract holds promise as a topical treatment to improve cosmetic skin quality.

Supplementary Materials: The following supporting information can be downloaded at https://www.mdpi.com/article/10.3390/cosmetics13060294/s1: Figure S1: Network analysis of DEGs in BoNT/A-treated explants; Figure S2: Network analysis of DEGs in α-bungarotoxin-treated explants; Figure S3: Network analysis of DEGs in myricetin-treated explants; Figure S4: Network analysis of DEGs in Blend 1-treated explants. Table S1: Differentially expressed genes in BoNT/A-treated explants; Table S2: Differentially expressed genes in α-bungarotoxin-treated explants; Table S3: Differentially expressed genes in myricetin-treated explants; Table S4: Differentially expressed genes in Blend 1-treated explants; Table S5: Downregulated DEG pairs between treatment conditions. Table S6: Upregulated DEG pairs between treatment conditions. Table S7: Gene list for heatmap clustering analysis.

Author Contributions: Conceptualization, H.K., R.J.B., R.Y.K., and S.K.; methodology, H.K., J.-W.M., R.J.B., and R.Y.K.; formal analysis, H.K., F.J., and R.J.B.; investigation, H.K., F.J., S.B., J.-W.M., and Y.N.; resources, D.-G.L., Y.M.H., J.-W.M., and C.-Y.H.; writing—original draft preparation, R.J.B.; writing—review and editing, R.J.B., H.K., F.J., and R.Y.K.; supervision, R.J.B. and R.Y.K.; project

administration, R.Y.K., S.K., and C.P. All authors have read and agreed to the published version of the manuscript.

Funding: This research was funded by L'Oréal Research & Innovation and Cosmax BTI; the funders had a role in the design of the study; in the collection, analysis and interpretation of the data; in the writing of the manuscript; and in the decision to publish the results, through the participation of their employees as authors, as detailed in the Author Contributions section. No external grant or funding number applies, as the work was financed internally by the companies.

Institutional Review Board Statement: The study was conducted in accordance with the Declaration of Helsinki and approved by the Institutional Review Board of Seoul National University Bundang Hospital, Seongnam, Republic of Korea (protocol code B-2201-732-302, approved on 23 December 2021).

Informed Consent Statement: Written informed consent was obtained from all donors of the human skin samples used in this study.

Data Availability Statement: The differentially expressed gene lists supporting the conclusions of this article are provided in the Supplementary Materials (Tables S1–S4). The underlying raw RNA sequencing data are not publicly available because they were generated from human skin explants under donor consent that does not permit the public release of individual-level sequence data, and because they relate to a proprietary cosmetic ingredient under commercial development. Requests to access the processed datasets should be directed to the corresponding author.

Acknowledgments: The authors thank Teng Yao of L'Oréal Research and Innovation China for her valuable advice on bulk transcriptomics. During the preparation of this manuscript, the authors used Google Gemini 2.5 Flash Image ("Nano Banana") for the purpose of generating draft artwork for the graphical abstract. ChatGPT Sol 6.1 was used to proofread the manuscript prior to submission. The authors have reviewed and edited the output and take full responsibility for the content of this publication.

Conflicts of Interest: H.K., Y.M.H., Y.N., D.G.L., and C.P. are employees of Cosmax BTI. S.K. is an employee of Cosmax. J.-W.M. is an employee of GFC. R.J.B., F.J., S.B., and R.Y.K. were all employees of L'Oréal Research & Innovation when the study was initiated. C.-Y.H. is a faculty member of Seoul National University Bundang Hospital and declares no competing financial interests. Blend 1 is a proprietary material under commercial development. This research was funded by L'Oréal Research & Innovation; the funder had a role in the design of the study; in the collection, analysis, and interpretation of the data; in the writing of the manuscript; and in the decision to publish the results, through the participation of its employees as authors, as detailed in the Author Contributions section.

References

1. Kumar, R.; Singh, B.R. Botulinum Toxin: A Comprehensive Review of Its Molecular Architecture and Mechanistic Action. *Int. J. Mol. Sci.* **2025**, *26*, 777. [CrossRef] [PubMed]
2. Pellett, S. Botulinum Neurotoxins: A Distinct Subclass of SNARE-Cleaving Endopeptidases. *Anaerobe* **2026**, *97*, 103035. [CrossRef] [PubMed]
3. Lou, X.; Shin, Y.-K. SNARE Zippering. *Biosci. Rep.* **2016**, *36*, e00327. [CrossRef] [PubMed]
4. Ayoub, N. Botulinum Toxin Therapy: A Comprehensive Review on Clinical and Pharmacological Insights. *J. Clin. Med.* **2025**, *14*, 2021. [CrossRef] [PubMed]
5. Bharadvaja, N.; Gautam, S.; Singh, H. Natural Polyphenols: A Promising Bioactive Compound for Skin Care and Cosmetics. *Mol. Biol. Rep.* **2023**, *50*, 1817–1828. [CrossRef] [PubMed]
6. Yang, Y.; Shin, J.Y.; Oh, J.-M.; Jung, C.H.; Hwang, Y.; Kim, S.; Kim, J.-S.; Yoon, K.-J.; Ryu, J.-Y.; Shin, J.; et al. Dissection of SNARE-Driven Membrane Fusion and Neuroexocytosis by Wedging Small Hydrophobic Molecules into the SNARE Zipper. *Proc. Natl. Acad. Sci. USA* **2010**, *107*, 22145–22150. [CrossRef] [PubMed]
7. Yang, Y.; Kim, S.-H.; Heo, P.; Kong, B.; Shin, J.; Jung, Y.-H.; Yoon, K.; Chung, W.-J.; Shin, Y.-K.; Kweon, D.-H. SNARE Zippering Is Hindered by Polyphenols in the Neuron. *Biochem. Biophys. Res. Commun.* **2014**, *450*, 831–836. [CrossRef] [PubMed]
8. Yang, Y.; Choi, J.K.; Jung, C.H.; Koh, H.J.; Heo, P.; Shin, J.Y.; Kim, S.; Park, W.-S.; Shin, H.-J.; Kweon, D.-H. SNARE-Wedging Polyphenols as Small Molecular Botox. *Planta Med.* **2012**, *78*, 233–236. [CrossRef] [PubMed]
9. Miean, K.H.; Mohamed, S. Flavonoid (Myricetin, Quercetin, Kaempferol, Luteolin, and Apigenin) Content of Edible Tropical Plants. *J. Agric. Food Chem.* **2001**, *49*, 3106–3112. [CrossRef] [PubMed]

10. Braun, S.; Croizat, B.; Lagrange, M.-C.; Warter, J.-M.; Poindron, P. Neurotrophins Increase Motoneurons' Ability to Innervate Skeletal Muscle Fibers in Rat Spinal Cord–Human Muscle Cocultures. *J. Neurol. Sci.* **1996**, *136*, 17–23. [CrossRef] [PubMed]
11. Filtjens, J.; Roger, A.; Quatrini, L.; Wieduwild, E.; Gouilly, J.; Hoeffel, G.; Rossignol, R.; Daher, C.; Debroas, G.; Henri, S.; et al. Nociceptive Sensory Neurons Promote CD8 T Cell Responses to HSV-1 Infection. *Nat. Commun.* **2021**, *12*, 2936. [CrossRef] [PubMed]
12. Liu, Z.; Bian, X.; Luo, L.; Björklund, Å.K.; Li, L.; Zhang, L.; Chen, Y.; Guo, L.; Gao, J.; Cao, C.; et al. Spatiotemporal Single-Cell Roadmap of Human Skin Wound Healing. *Cell Stem Cell* **2025**, *32*, 479–498.e8. [CrossRef] [PubMed]
13. Qu, H.-Q.; Kao, C.; Hakonarson, H. Implications of the Non-Neuronal Cholinergic System for Therapeutic Interventions of Inflammatory Skin Diseases. *Exp. Dermatol.* **2024**, *33*, e15181. [CrossRef] [PubMed]
14. Stegemann, A.; Böhm, M. Targeting the α7 Nicotinic Acetylcholine Receptor—A Novel Road towards the Future Treatment of Skin Diseases. *Exp. Dermatol.* **2020**, *29*, 924–931. [CrossRef] [PubMed]
15. Kurzen, H.; Schallreuter, K.U. Novel Aspects in Cutaneous Biology of Acetylcholine Synthesis and Acetylcholine Receptors. *Exp. Dermatol.* **2004**, *13*, 27–30. [CrossRef] [PubMed]
16. Foulad, D.P.; Cirillo, N.; Grando, S.A. The Role of Non-Neuronal Acetylcholine in the Autoimmune Blistering Disease Pemphigus Vulgaris. *Biology* **2023**, *12*, 354. [CrossRef] [PubMed]
17. Stegemann, A.; Flis, D.; Ziolkowski, W.; Distler, J.H.W.; Steinbrink, K.; Böhm, M. The α7 Nicotinic Acetylcholine Receptor: A Promising Target for the Treatment of Fibrotic Skin Disorders. *J. Investig. Dermatol.* **2020**, *140*, 2371–2379. [CrossRef] [PubMed]
18. Breton, L.; De Azevedo Calderon, L.; Zanchi, F.; Ferreira Francisco, A.; De Vecchi, R. Bioactive Peptides Having High Binding Affinity to Human Muscular Nicotinic Acetylcholine Receptor. European Patent EP3787660A1, 10 March 2021.
19. Brandt, F.; O'Connell, C.; Cazzaniga, A.; Waugh, J.M. Efficacy and Safety Evaluation of a Novel Botulinum Toxin Topical Gel for the Treatment of Moderate to Severe Lateral Canthal Lines. *Dermatol. Surg.* **2010**, *36*, 2111–2118. [CrossRef] [PubMed]
20. Mahmoud, B.H.; Burnett, C.; Ozog, D. Prospective Randomized Controlled Study to Determine the Effect of Topical Application of Botulinum Toxin A for Crow's Feet after Treatment with Ablative Fractional CO_2 Laser. *Dermatol. Surg.* **2015**, *41*, S75–S81. [CrossRef] [PubMed]
21. Cao, Y.; Yang, J.-P.; Zhu, X.-G.; Zhu, J.; Chang, H.-Q.; Guo, S.-H.; Luo, D.; Zhou, B.-R. A Comparative In Vivo Study on Three Treatment Approaches to Applying Topical Botulinum Toxin A for Crow's Feet. *BioMed Res. Int.* **2018**, *2018*, 6235742. [CrossRef] [PubMed]
22. Ebrahim, H.; Elardi, A.; Khater, S.; Morsi, H. Successful Topical Application of Botulinum Toxin after Microneedling versus Microneedling Alone for the Treatment of Atrophic Post-Acne Scars: A Prospective, Split-Face, Controlled Study. *J. Clin. Aesthet. Dermatol.* **2022**, *15*, 26–31. [PubMed]
23. Nguyen, T.T.M.; Yi, E.-J.; Jin, X.; Zheng, Q.; Park, S.-J.; Yi, G.-S.; Yang, S.-J.; Yi, T.-H. Sustainable Dynamic Wrinkle Efficacy: Non-Invasive Peptides as the Future of Botox Alternatives. *Cosmetics* **2024**, *11*, 118. [CrossRef]
24. Debono, J.; Xie, B.; Violette, A.; Fourmy, R.; Jaeger, M.; Fry, B.G. Viper Venom Botox: The Molecular Origin and Evolution of the Waglerin Peptides Used in Anti-Wrinkle Skin Cream. *J. Mol. Evol.* **2017**, *84*, 8–11. [CrossRef] [PubMed]
25. Trookman, N.S.; Rizer, R.L.; Ford, R.; Ho, E.; Gotz, V. Immediate and Long-Term Clinical Benefits of a Topical Treatment for Facial Lines and Wrinkles. *J. Clin. Aesthet. Dermatol.* **2009**, *2*, 38–43. [PubMed]
26. Favreau, P.; Benoit, E.; Hocking, H.G.; Carlier, L.; Hoedt, D.D.; Leipold, E.; Markgraf, R.; Schlumberger, S.; Córdova, M.A.; Gaertner, H.; et al. A Novel μ-Conopeptide, CnIIIC, Exerts Potent and Preferential Inhibition of NaV1.2/1.4 Channels and Blocks Neuronal Nicotinic Acetylcholine Receptors. *Br. J. Pharmacol.* **2012**, *166*, 1654–1668. [CrossRef] [PubMed]
27. Heo, P.; Park, J.-B.; Shin, Y.-K.; Kweon, D.-H. Visualization of SNARE-Mediated Hemifusion between Giant Unilamellar Vesicles Arrested by Myricetin. *Front. Mol. Neurosci.* **2017**, *10*, 93. [CrossRef] [PubMed]
28. Heo, P.; Yang, Y.; Han, K.Y.; Kong, B.; Shin, J.-H.; Jung, Y.; Jeong, C.; Shin, J.; Shin, Y.-K.; Ha, T.; et al. A Chemical Controller of SNARE-Driven Membrane Fusion That Primes Vesicles for Ca^{2+}-Triggered Millisecond Exocytosis. *J. Am. Chem. Soc.* **2016**, *138*, 4512–4521. [CrossRef] [PubMed]
29. Schlereth, T.; Birklein, F.; Haack, K.; Schiffmann, S.; Kilbinger, H.; Kirkpatrick, C.J.; Wessler, I. In Vivo Release of Non-Neuronal Acetylcholine from the Human Skin as Measured by Dermal Microdialysis: Effect of Botulinum Toxin. *Br. J. Pharmacol.* **2006**, *147*, 183–187. [CrossRef] [PubMed]
30. Bukharaeva, E.A.; Skorinkin, A.I.; Samigullin, D.V.; Petrov, A.M. Presynaptic Acetylcholine Receptors Modulate the Time Course of Action Potential-Evoked Acetylcholine Quanta Secretion at Neuromuscular Junctions. *Biomedicines* **2022**, *10*, 1771. [CrossRef] [PubMed]
31. Novo Pereira, I.; Canales, G.D.l.T.; Durão, S.; Shado, R.; Braga, A.C.; Almeida, A.M.; Hassan, H.; Manso, A.C.; Faria-Almeida, R. Botulinum Toxin Effects on Biochemical Biomarkers Related to Inflammation-Associated Head and Neck Chronic Conditions: A Systematic Review of Preclinical Research. *Toxins* **2025**, *17*, 377. [CrossRef] [PubMed]
32. Jung, D.; Shin, S.M.; Kim, K.H.; Kim, K.J.; Park, E.J. Botulinum Toxin A Modulates Keratinocyte Proliferation and Inflammatory and Pruritic Mediators in Wound Healing. *Ann. Dermatol.* **2025**, *37*, 269–275. [CrossRef] [PubMed]

33. Han, S.B.; Kim, H.; Cho, S.H.; Chung, J.H.; Kim, H.S. Protective Effect of Botulinum Toxin Type A against Atopic Dermatitis-Like Skin Lesions in NC/Nga Mice. *Dermatol. Surg.* **2017**, *43*, S312–S321. [CrossRef] [PubMed]
34. Dağtaş, B.B.; Erdem, O.; Güneç, T.İ.; Avcı, E.B.; Manav, V.; Koku Aksu, A.E. Effects of Botulinum Toxin Type A Treatment on Clinical and Biophysical Parameters in Patients with Erythematotelangiectatic Rosacea: A Prospective, Randomized, Controlled, Double-Blind Study. *Dermatol. Surg.* **2025**, *51*, 515–521. [CrossRef] [PubMed]
35. Meng, J.; Wang, J.; Buddenkotte, J.; Buhl, T.; Steinhoff, M. Role of SNAREs in Atopic Dermatitis-Related Cytokine Secretion and Skin-Nerve Communication. *J. Investig. Dermatol.* **2019**, *139*, 2324–2333. [CrossRef] [PubMed]
36. Wang, N.; Dong, Y.; Xu, X.; Shen, Y.; Huang, Z.; Yu, Y.; Liu, Z.; Gong, W.; Zhang, S.; Zheng, Y.; et al. Fibroblast Growth Factor 10 Protects against UVB-Induced Skin Injury by Activating the ERK/YAP Signalling Pathway. *Cell Prolif.* **2022**, *55*, e13315. [CrossRef] [PubMed]
37. Basalova, N.; Alexandrushkina, N.; Grigorieva, O.; Kulebyakina, M.; Efimenko, A. Fibroblast Activation Protein Alpha (FAPα) in Fibrosis: Beyond a Perspective Marker for Activated Stromal Cells? *Biomolecules* **2023**, *13*, 1718. [CrossRef] [PubMed]
38. Krawetz, R.J.; Abubacker, S.; Leonard, C.; Masson, A.O.; Shah, S.; Narendran, N.; Tailor, P.; Regmi, S.C.; Labit, E.; Ninkovic, N.; et al. Proteoglycan 4 (PRG4) Treatment Enhances Wound Closure and Tissue Regeneration. *npj Regen. Med.* **2022**, *7*, 32. [CrossRef] [PubMed]
39. Mestrallet, G.; Rouas-Freiss, N.; LeMaoult, J.; Fortunel, N.O.; Martin, M.T. Skin Immunity and Tolerance: Focus on Epidermal Keratinocytes Expressing HLA-G. *Front. Immunol.* **2021**, *12*, 772516. [CrossRef] [PubMed]
40. Pérez, L.A.; León, J.; López, J.; Rojas, D.; Reyes, M.; Contreras, P.; Quest, A.F.G.; Escudero, C.; Leyton, L. The GPI-Anchored Protein Thy-1/CD90 Promotes Wound Healing upon Injury to the Skin by Enhancing Skin Perfusion. *Int. J. Mol. Sci.* **2022**, *23*, 12539. [CrossRef] [PubMed]
41. Jung, S.K.; Lee, K.W.; Kim, H.Y.; Oh, M.H.; Byun, S.; Lim, S.H.; Heo, Y.-S.; Kang, N.J.; Bode, A.M.; Dong, Z.; et al. Myricetin Suppresses UVB-Induced Wrinkle Formation and MMP-9 Expression by Inhibiting Raf. *Biochem. Pharmacol.* **2010**, *79*, 1455–1461. [CrossRef] [PubMed]
42. Lin., T.-C.; Yang, C.-Y.; Wu, T.-H.; Tseng, C.-H.; Yen, F.-L. Myricetin Nanofibers Enhanced Water Solubility and Skin Penetration for Increasing Antioxidant and Photoprotective Activities. *Pharmaceutics* **2023**, *15*, 906. [CrossRef] [PubMed]

Disclaimer/Publisher's Note: The statements, opinions and data contained in all publications are solely those of the individual author(s) and contributor(s) and not of MDPI and/or the editor(s). MDPI and/or the editor(s) disclaim responsibility for any injury to people or property resulting from any ideas, methods, instructions or products referred to in the content.